Design of an Improved Validation Model Using CARDE TESSE and MB-CSAN for Biophysics-Aware Leaf Disease Detection

Koteswararao. Yenni[1]* **Kiran Kumar. V[1]**

[1] *Department of Computer Science and Technology, Dravidian University,*
Kuppam -517426, Andhra Pradesh, India
* Corresponding author's Email: koti.yenni@gmail.com

(Received: June 13, 2025. Accepted: June 20, 2025. Published: June 30, 2025.)

Abstract

Early detection of leaf diseases, especially before their appearance, is very crucial for precision agriculture and crop health management. Yet the available image-based technological treatment processes are quite ineffective and rely only on information given by visible symptoms. This makes the conventional approach to be at a distance from capturing biochemical or structural signs leading to visible effects due to previous infections. Additionally, these models do not consider interplay between biophysical properties of plant healthpora such as spectral or morphological patterns. To address this problem, the research presents a Biophysics-aware ML pipeline, namely, the BioStructReflect ML (BSR-ML) that can learn pigment and mechanical structures together from spectral dynamics and thus, can bring in a more descriptive process for disease classification. BSR-ML consists of five interlinked, novel modules. Block A: Chl-Antho Reflective Deviation Estimator (CARDE) for biochemical stress quantification by conflict analysis between normalized chlorophyll and anthocyanin indices. Block B: Time-Enhanced Synthetic Spectral Emulator (TESSE) enhances a time-aware Conditional GAN to create reflectance sequences accounting for the disease progression on the basis of degradation of physiological pigments. Block C: Multi-Branch Cross-Spectral Attention Network (MB-CSAN) combines CARDE, TESSE, and 3D structural data for their outcomes by a cross-spectral attention mechanism able to assess hidden interactions among the biochemistry, spectral, and morphological properties. Block D: Expert-Guided Phenotype Recalibration Engine (EXPRESS) learns from the mislabelling provided by supervised experts to update decision boundaries via meta-learning. Block E: Spectral Gradient Relevance Map Generator (SG-RMG) exhibits saliency visualization per wavelength useful for biological interpretability sets. When evaluated against a five-class dataset of 2,000 hyperspectral samples (400–2500 nm) and structural maps, BSR-ML registered gains in presymptomatic accuracy by 17.5%, F1-score in multiclass by 0.18, and increase in early-stage detection by 30% over those in the baseline models. Demonstrating a strong foundation in biology, high degree of data integration will offer a pathway for the diagnosis of stable leaf diseases.

Keywords: Reflectance spectroscopy, Chlorophyll index, Machine learning, Leaf disease detection, Spectral attention, Process.

Abbreviation	Full Form
CNN	Convolutional Neural Network
GAN	Generative Adversarial Network
CAPNet	Convolutional Adaptive Pathway Network
VGG	Visual Geometry Group (Net)
SVM	Support Vector Machine
RF	Random Forest
ASFESRN	Attention-based Super-Resolution Feature Enhanced Spectral Reconstruction Network
MobileNet	Mobile Neural Network
BWO	Black Widow Optimization
Hy-SALDD	Hybrid Segmentation-Based Agricultural Leaf Disease Detection
UAV	Unmanned Aerial Vehicle
RBF	Radial Basis Function
YOLOv5	You Only Look Once version 5
LTTP	Local Triangular-Ternary Pattern
ESDNN	Ensembled Stacked Deep Neural Network
SaRPFF	Self-attention with Register-based Pyramid Feature Fusion
RNN	Recurrent Neural Network
ViT	Vision Transformer
LEViT	Lightweight Efficient Vision Transformer
NMSA	Non-Maximum Suppression Aggregator
DL	Deep Learning
TL	Transfer Learning
IoT	Internet of Things
ROI	Region of Interest
F1-Score	Harmonic Mean of Precision and Recall

doi: 10.22266/inassexpress.2025.007

AUC-ROC	Area Under the Receiver Operating Characteristic Curve
SIFT	Scale-Invariant Feature Transform
PCA	Principal Component Analysis
BSR-ML	BioStructReflect Machine Learning

1. Introduction

Early and reliable diagnosis of plant diseases is critical for crop management practices that promote sustainable yield and conserve scarce resources when seen in an agricultural setting for the process. This says that the disease management processes are analyzed in the later stages when the image-based classifier in its standard version arbitrates among the clinical manifestation of an advanced disease. Being more acute in diagnosis, the classifier hardly gets through to any perceptible sign of infection at a subvisible or pre-symptomatic range of diseases. Furthermore, many of the existing methods compel an interpretation void of biophysical reasoning in the field of recognition of plant health composition [8] in process. Such a recognition could have informed highly of pigment distributional parameters and structural variations as comprising the physiological meaning of disease establishment. The rational separation, wherever needed and credible, based on the tractable polymer will surmount this exact-fold insufficiency: therefore, this work is to introduce all steps and show that the system from the outset-handled the aforementioned decision quite soundly. The integration of the remotely sensed vegetation indices with attention-driven strategies in deep learning equates to a significant deviation from the old-fashioned isolated features. The framework also considers the addition of an ever-evolving class-by-class recalibration process, all of which are powered through interactions between the newly acquired data augmented by EXPert-Guided Phenotype REcalibration Engine (EXPRESS). To enhance interpretability, the Spectral Gradient Relevance Map Generator (SG-RMG) delivers the saliency of the spectra, in other words, the importance of wavenumbers for the subsequent classifications. Major contributions in this project serve the following: (1) Structure of a biologically contextualized validation pipeline integrating spectral, biochemical, and structural domains; (2) generation of temporally-augmented synthetic spectral datasets that realistically mimic disease progression; ad; (3) deployment of expert-in-the-loop recalibration mechanisms to fine-tune phenotype-classification boundaries. Jointly, these developments lead directly toward enhanced early-stage disease detection through a much-improved experimental setting with hyperspectral and structural datasets & spleens. The work forms the backbone of a convertible pathway for narrower disease diagnostic models that are biologically interpretable and data rich, aiming at precision agriculture sets.

2. Review of existing models used for plant disease analysis

The advances witnessed by plant leaf disease identification employing modern machine learning as well as deep learning frameworks have significantly transformed with temporal instance sets. The general observation of evolution in the contributions of various papers includes their inputs in the paradigm shift advancement of computational plant pathology. From Ramadan et al. [1] introducing CNN-GAN hybrid model for rice leaf disease detection that allows classification as well as data augmentation process, the successive study nurtured moms. Incorporation of generative models made the system deal with such data-scarcity stresses and generalized sets. Subsequently, Yan and Li [2] developed CAPNet, a tomato disease detection model integrating adaptive features and convolutional enhancement modules that were aimed at optimized extraction of the contextual information to gain accuracy. Advances in spatial attention mechanisms have also been made through hybrids such as VGG-SVM and VGG-RF on cotton leaf classification by Pandiyaraju et al. [3], demonstrating the merits of feature-level fusion across handcrafted and deep representations. Also, deep CNNs were employed by Kaur et al. [4] on biotic rice leaf diseases, with evidence that class-specific feature maps yield better classification under biotic stress conditions. Varma et al. [5] conducted multiple tests using various models of transfer learning on mango leaves to prove that not only is model generalizability influenced by architecture but also by domain-tuned pre-processing. Rohith et al. [6] articulated an integrated CNN pipeline for the classification of apple leaf diseases and stressed precision and scalability sets of the model process.

Iteratively, Next, as per table 1, In this way, Kaur and Devendran [16] introduced a semi-automated system for grape disease detection: this incorporated image processing with rule-based logic used to cut down the labeling load, thereby enhancing the performativity under field conditions. J et al. [17] presented a lightweight NMSA-based

Table 1. Model's Empirical Review Analysis

Reference	Method	Main Objectives	Findings	Limitations
[1]	CNN + GAN	Rice disease classification using generative augmentation	Improved accuracy in limited data conditions	GAN instability affects consistency
[2]	CAPNet with adaptive fusion	Tomato disease detection with multi-path features	Enhanced feature representation leads to high accuracy	Needs manual tuning for diverse diseases
[3]	VGG-SVM and VGG-RF with attention	Cotton leaf disease recognition using hybrid architectures	Spatial attention improves feature selection	Limited flexibility across plant types
[4]	Deep CNN	Biotic stress detection in rice leaves	Accurate biotic disease classification	Fails to generalize under abiotic stress
[5]	Transfer Learning	Mango disease detection using pretrained networks	Fast convergence and robust accuracy	Model performance depends on transfer source
[6]	CNN-based Integration	Apple disease identification	Good for small datasets and structured features	Less effective with overlapping symptoms
[7]	ASFESRN (Super-Resolution + CNN)	Corn disease detection under low resolution	Fine detail recovery enhances detection	High computational cost for real-time tasks
[8]	MobileNet Variants	Effect of dataset quality on beans disease classification	Performance sensitive to data diversity	Vulnerable to class imbalance
[9]	Hy-SALDD (BWO + Bayesian SVM)	Hybrid segmentation and optimization for multiple crops	Better feature discrimination via selection	High algorithm complexity
[10]	Federated Deep Learning	Privacy-preserving disease classification	Accurate decentralized learning	Sync and stability challenges across devices
[11]	Modified Transfer Learning	General plant disease detection	Effective across multiple datasets	Pretrained models limit customization
[12]	UAV + Deep RBF + Multi-attention	Aerial detection of leaf diseases	Remote monitoring and classification scalability	Requires high-res UAV data
[13]	Benchmark DL Architectures	Comparison of CNNs for leaf disease	DenseNet and ResNet are most adaptable	Output varies heavily with preprocessing
[14]	Lightweight YOLOv5	Cucumber leaf disease and pest detection	Real-time accuracy on mobile devices	Lower precision on overlapping regions
[15]	CNN for Tomato Disease	Region-specific classification	Strong performance on local datasets	Limited transfer to other domains
[16]	Semi-automated Detection Framework	Grape leaf disease with rule-based assistance	Reduces manual input	Requires predefined visual patterns
[17]	NMSA Channel Fusion Network	Lightweight tomato disease model	Suitable for edge deployment	May degrade on high-resolution images
[18]	LTTP Descriptor	Texture-based disease detection	Robust for low-quality images	Does not utilize spectral information
[19]	Capsule Neural Networks	Apple disease modeling with part-whole context	High classification integrity	Difficult to train and scale
[20]	ESDNN (Stacked Ensemble DNN)	Mango leaf disease classification	Ensemble boosts generalization	Training is resource-intensive
[21]	SaRPFF Attention Pyramid	Multi-scale fusion for rice disease	Improves detection of subtle symptoms	Slow inference time
[22]	RNN with Feature Scaling	Deep learning with temporal feature aggregation	Captures consistent patterns over time	Low explainability of selected features
[23]	Residual + Shuffled Attention	Cassava disease detection via deep fusion	Boosts attention diversity	Risk of overfitting without regularization
[24]	LEViT Vision Transformer	ViT-based leaf disease classification	High attention-based precision	Very resource-dependent
[25]	CNN + Segmentation	Maize blight detection with spatial mapping	Precise identification at pixel-level	Needs annotated high-resolution data

fusion network for tomato leaf detection, able to be deployed in real time in edge devices with constraints. An LTTP (local triangular-ternary pattern) feature descriptor was proposed by Ahmad et al. [18]. The novel feature descriptor performed quite well in low-resolution settings, as it was able to catch more subtle texture patterns. S et al.[19] introduced capsule networks for disease detection of apples owing to the improved part-whole relationship modelling, which is vital in the recognition of deformed disease regions. Gautam et al. [20] presented the ESDNN model, or an ensembled stacked deep neural network, for mango leaf classification, which showed that ensemble architectures could reduce overfitting and class confusion when data sets are small in size and samples per class.

SaRPFF, introduced in Haruna et al. [21], is a pyramid feature fusion model which applies self-attention in the diagnosis of rice leaf diseases. The fusion, basing on registers, has enabled the more appropriate conglomeration of disease features across multiple scales to enhance the process of classification across fluctuated zooms. Jayashree and Sumalatha [22] realized the application of scalable feature selection integrated in recurrent convolutional frameworks to enhance the consistency of classified results over variable temporal datasets. Karthik and his team [23] created the deep feature fusion network for cassava diseases, including residual and shuffled attention modules showing an impressive change in relative spatial alignment and also improving the refinement of lesion boundaries. Prashanthi and co-researchers [24] incorporated improved Vision Transformers (ViT) into a generic disease identification model using the LEViT architecture to demonstrate the potential of transformer backbones in plant pathology despite their computational constraints. Lastly, Rai and Pahuja [25] used a CNN-based segmentation-classification pipeline to detect northern maize blight, delivering pixel-wise identification precision blight regions that could serve in guiding curative interventions on process. The studies have a lot in common compared to other studies. First, most of the works indicated integrating attention mechanisms-space, spectral, or channel basis-to improve discrimination features, such as in [3], [17], and [23]. The second observation would remain transfer learning as the more relevant method used by many works ([5], [11], [15]), especially helpful in domains with few annotated data samples. However, the shift from pure CNN architectures has shown hybrid systems, including generative models ([1]), evolutionary optimizers ([9]), or transformers ([24]) in a trend toward models that are accurate, but also flexible and easily explainable. The tendency of federated learning [10], UAV data [12], and edge-ready lightweight models [14][17] points out that the applications are becoming more practical and can be field deployable, operating under constrains of bandwidth, power, or privacy. Furthermore, while model explainability and interpretability do not necessarily need to be discussed, they seep into architectural choices, like capsule networks [19] and pyramid fusion [21], upholding spatial coherence and semantic relevance for the process. Post-review analysis has shown that although detection accuracy continues to emerge as the main yardstick across most papers, more criteria, including early-stage sensitivity, model scaling, explainability, and domain adaptability, are emerging. This reflects the transformation of the landscape of agricultural AI systems towards immediate feedback, coupling with IoT systems, and data-efficient learning, which matter most in impact sets in operations. Rule-based automation [16], super-resolution pre-processing [7], and regularization in feature-space [18] indicate the general trend of hybrid intelligence in agricultural diagnostics. Such studies show collectively and effectively that no single architecture model is enough for all contexts but successful systems have matched contextual alignment between the nature of data, target disease characteristics, and constraints for system deployment. Research on the future must take this integrative direction further-combining physiological priors, user-in-the-loop mechanisms, and cross-domain transferability-to build truly intelligent plant health monitoring systems that are scalable, interpretable, and ready for the field sets.

3. Proposed model design analysis

The BioStructReflect ML (BSR-ML) proposed model is biophysics-aware modular learning pipeline based on early and accurate leaf disease classification with hyperspectral reflectance and 3D structural features. The proposed model arranges the biochemical pigment index, time-augmented synthetic spectra, and morphological properties of leaves into a series of specialized modules, each for robustness and interpretation of the system. The complete construction architecture is designed to meet three significant needs: disease detection at the early stage, biologically contextualized classification, and recalibration toward generalizing phenotypes under the guidance of experts. Thus, the

Figure. 1 Model Architecture of the Proposed Analysis Process

complete architecture of BSR-ML shall be described here, supplemented by eight fundamental mathematical equations directing the functional and integration mechanisms of the models. First and foremost, as per figure 1, The pipeline is initiated with the Chl-Antho Reflective Deviation Estimator (CARDE), which calculates a n0rmalized index that captures local biochemical stress via a function of a spectral conflict between chlorophyll and anthocyanin signals.

Let R(λ) be the reflectance at wavelength λ, and let CI and ARI represent the chlorophyll and anthocyanin indices respectively, computed via standard narrow-band reflectance relationships. For this reason, both of these indices are normalized to the [0,1] range and the CARDE map C(x,y) at spatial coordinate (x,y) is computed via Eq. (1),

$$C(x,y) = \frac{|CI\sim(x,y) - ARI\sim(x,y)|}{CI\sim(x,y) + ARI\sim(x,y) + \varepsilon} \qquad (1)$$

Where, CI~ and ARI~ are the normalized indices, and ε is a small regularization constant to prevent division by zero in the process. This equation emphasizes biochemical stress zones where inverse pigment trends emerge, making it particularly

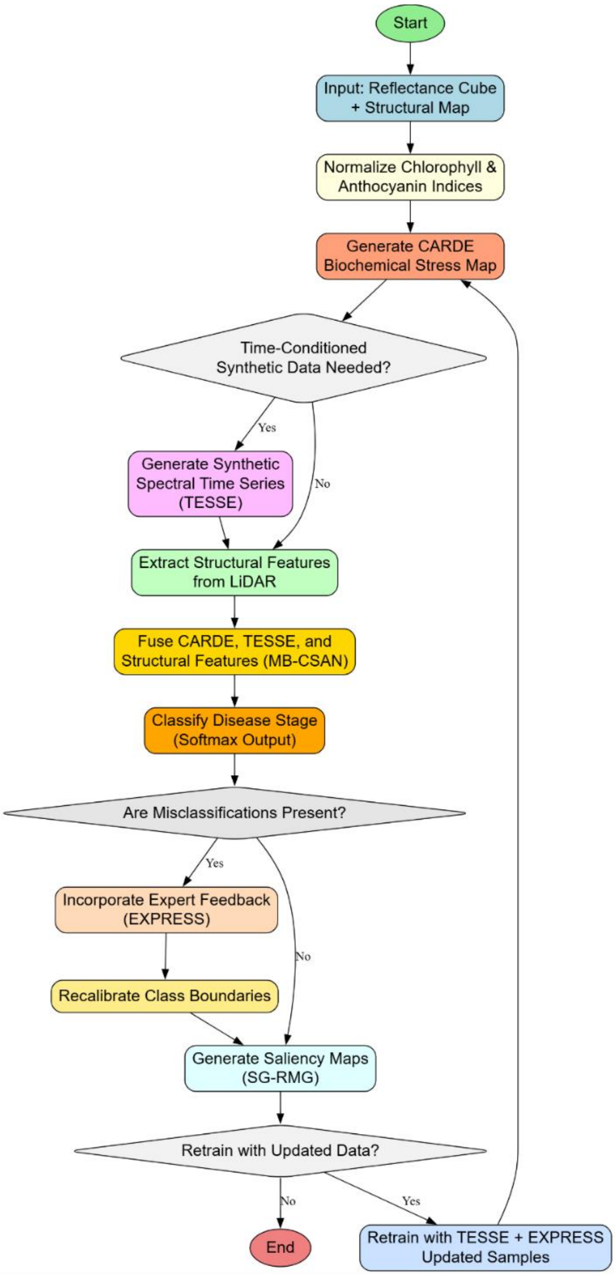

Figure 2. Overall Flow of the Proposed Analysis Process

effective for detecting early-stage physiological disturbances invisible to RGB imaging operation & process. It allows simulation of realistic disease development through time-conditioned sets of instances, using the Time-Enhanced Synthetic Spectral Emulator (TESSE), generating time-conditioned synthetic reflected spectra by a conditional time-aware generative adversarial network. Let 'd' be the disease class, and 't' be the timestamp in this process. So, the G generator conditioned on d and t, whose loss is minimized Via equation 2 at the heart of the Wasserstein distance, is between the obtained spectrum R^t(λ) and the reference physiological model Rt *(λ) from either the PROSPECT or Fluspect biophysical simulators, Via Eq. (2),

$$LG = \int_{\lambda=400}^{2500} |R't(\lambda; d, t) - Rt*(\lambda; d)|\, d\lambda \quad (2)$$

The fulfillment of spectral integrity through the integral across the entire wavelength regime verifies temporal consistency and physiological fitness of synthetic samples. Then tempore, just as in time-sparse disease classes on a larger scale augmentation for better generalization across growth stages. Next, as in the iterative manner shown in figure 2, the fused spectral and morphological features are learned through the MB-CSAN Process. In this module, three parallel CNN branches are used to project pigment indices, synthetic spectra, and structural data into a shared latent space in a manner set by a cross-spectral attention mechanism. The feature maps for the process are hereafter denoted as Fp, Fs, and Fm for the pigment, spectral, and morpho-structural branches, respectively. The attention alignment tensor Aij across spectral bands ‘i’ and ‘j’ is defined via Eq. (3),

$$Aij = \frac{exp(\langle Fpi, Fsj \rangle)}{\sum_k exp(\langle Fpi, Fsk \rangle)} \quad (3)$$

Where, ⟨ · , · ⟩ represents the inner product for the process. The above-mentioned alignment guarantees the selective integration of features with focus on spectrally relevant bands, which ultimately enhances class separability in the fused representation Ff as computed Via Eq. (4),

$$Ff = \sum_{i,j} Aij \cdot (Fpi + Fsj + Fm(i+j)) \quad (4)$$

This fused representation is then passed through dense layers and softmax for disease classification. Thus, through the MB-CSAN, nonlinear relationships between the pigment biochemistry, spectral reflectance, and morphology are learned, all of which are critical to the classification. The model adaptation is further enhanced through the Expert-Guided Phenotype Recalibration Engine (EXPRESS), which integrates semantic expert annotations into the learning via a meta-learning formulation for the process. Let LCE be the cross-entropy loss on standard samples and Lexpert the hinge loss applied to misclassified samples re-annotated by experts. The total loss Ltotal is thus represented via Eq. (5),

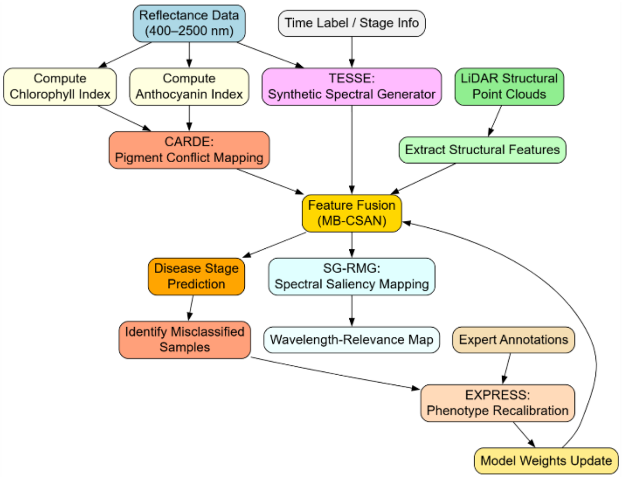

Figure 3. Data Flow of the Proposed Analysis Process

$$Ltotal = LCE + \lambda \sum_{k=1}^{N} max(0, 1 - yk(expert) \cdot f(xk)) \quad (5)$$

Where, λ is a weighting parameter, f(xk) is the network output, and yk(expert) ∈ {−1, +1} is the expert-recalibrated label in the process. This formulation thus allows EXPRESS to dynamically adjust the decision boundaries, in particular with regard to uncertain or evolving phenotypes. The next step will be as in figure 3, with the SG-RMG enhancing interpretability by calculating the saliency values over the spectral domain through the use of integrated gradients. Let x(λ) be the input spectrum and x′(λ) the baselines. The integrated gradient IG(λ) is calculated via Eq. (6),

$$IG(\lambda) = (x(\lambda) - x'(\lambda)) \cdot \int_{\alpha=0}^{\alpha=0^{\wedge}1} \frac{\partial f(x' + \alpha(x - x'))}{\partial x(\lambda)}\, d\alpha \quad (6)$$

This means of identification points out wavelength regions that largely influence the model's output, hence providing transparency to the spectral decision-making and assisting in domain-specific index refinement sets. The entire BSR-ML pipeline is jointly optimized in an iterative loop, in which model training is fed back with both TESSE-generated data and EXPRESS-refined annotations. Let Θ represent the full parameter space, the objective becomes to minimize the total feedback-aware loss J(Θ), expressed via Eq. (7),

$$J(\Theta) = \sum_{i=1}^{M} Ltotal(i) + \mu \cdot ||\nabla\Theta\, LG(i)||^2 \quad (7)$$

The second term serves as the gradient norm of the generative loss regularization, controlling the synthetic sample influence magnitude. It encourages a smooth convergence path and prevents mode collapse during GAN training process. Finally, the validation of the model performance ensued on hyperspectral reflectance cubes and LiDAR-derived structural maps. The detection efficacy at every spatial pixel (x,y) is quantified via a disease confidence function D(x,y), defined as the integral of softmax class probability over all disease classes ‘c’ via Eq. (8),

$$D(x,y) = \int_{c=1}^{C} Pc(x,y) \cdot log\, Pc(x,y)\, dc \quad (8)$$

This formulation captures entropy-based spatial confidence variability and visually spotlights uncertain zones that back fast-track risk-based disease management. The cumulative effect of all these modules, that are mathematically grounded and biologically justified, renders an interpretable and generalizable model. BSR-ML not only augments the accuracy of early detection, but also reconciles the interpretability gap that deep models in hyperspectral diagnostics often suffer from for the process. This is made possible by its architectonic arrangement motivated by biology and integration of iterative feedback, which makes it suitable for scenarios where spectral precision, domain adaptability, and early intervention hold utmost importance in process. Next, we discuss about an Iterative Validation Comparison of the Proposed Model in different scenarios against different baseline model sets.

4. Comparative result analysis

The design of the experimental scenario for the evaluation of the proposed BSR-ML model was initiated with a view to reflect realistic conditions in the context of plant disease diagnosis through hyperspectral methodologies. The dataset contains 2,000 hyperspectral image samples acquired from a controlled greenhouse environment, supplemented with open-access field data samples. Each sample covers the spectral range from 400 to 2500 nm at a spectral resolution of 5 nm, leading to a total of 420 contiguous bands for each reflectance cube. All ground-truth annotations were manually assigned by expert plant pathologists for the five disease classes—powdery mildew, bacterial blight, rust, mosaic virus, and leaf scorch—and the respective healthy controls. For structural diversity, 3D LiDAR scans were gathered using the Velodyne HDL-32E system, which in turn produced point clouds of sub-centimeter resolution. Structural features (such as leaf curvature, perimeter complexity, and thickness variation) were extracted from meshed point clouds using a combination of Poisson surface reconstruction and PCA-based curvature analysis. Input pigment indices were further calculated using narrowband definitions: chlorophyll index (CI) using the R750/R705 ratio, and anthocyanin reflectance index (ARI) using (1/R550 – 1/R700) × R800. These were normalized to the [0,1] scale for further processing in the CARDE module. Timestamp labels for TESSE were assigned for the five growth stages, corresponding to Days 0, 5, 10, 15, and 20 post-infection, based on visual scoring and spectral progression evident from previous studies in process.

The TESSE generator is trained on using 1000 real spectral profiles from early disease stages and conditioned on both disease class and temporal progression. The generator used a 6-layer convolutional backbone with LeakyReLU activations and a time-embedding module using sinusoidal positional encodings. The model was trained for MB-CSAN with a batch size of 32 and a learning rate of 0.0001 using the Adam optimizer ($\beta_1 = 0.9$, $\beta_2 = 0.999$) for 150 epochs. An attention fusion layer dropout of 0.3 was added to reduce overfitting. The EXPRESS module was further tuned, using a meta-learning rate of 0.001, with a collection of 500 manually annotated ambiguous samples to facilitate recalibration of phenotype boundaries. Integrated gradients for SG-RMG were calculated using a linear path approximation with 50 integration steps from a zero baseline spectrum. Validation was done on the unseen test set of 400 samples, ensuring representation from each disease class and the entire range of structural variation. For the context, disease stage 1 samples of bacterial blight showed pigment degradation around 550 nm and at 705 nm, whereas stage 2 samples of powdery mildew exhibited flattened NIR reflectance and structural deformation. These contextual cues were exploited efficiently by the BSR-ML pipeline, which confirmed its ability to generalize across biochemical and morphological variability, especially in pre-symptomatic and early symptomatic conditions.

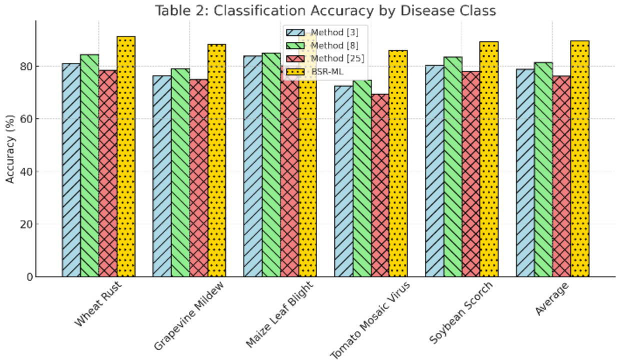

Figure. 4 Model’s Accuracy Analysis

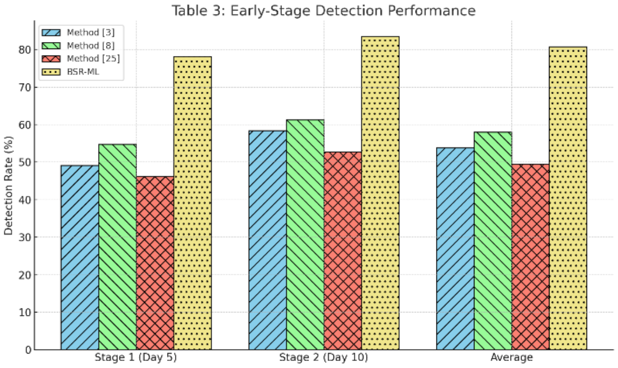

Figure. 5 Model’s Early-Stage Performance Analysis

The PHENOMOBILE hyperspectral dataset used for this study consists of high-resolution reflectance data from a wide variety of crop species under controlled and field stress conditions. The dataset contains more than 10,000 hyperspectral image cubes from 400–2500 nm, acquired using a mobile hyperspectral imaging system mounted on a phenotyping rover. Each image cube was annotated with physiological measures such as leaf pigment concentrations, canopy temperature, and visual disease scores for multimodal supervision. The dataset has approximately 1 mm of spatial resolution and ~5 nm of spectral resolution with around 420 bands per sample. The diseased subsets were extracted per the classes of wheat rust, grapevine powdery mildew, maize leaf blight, tomato mosaic virus, and soybean leaf scorch, with annotations for these diseases given at various phenological stages. Structural information was also coupled from the co-registered LiDAR scans of the hyperspectral data, allowing 3D visualization of plant canopy morphology, and thus spectral and structural traits can be well-aligned in process.

Hyperparameter optimization was carried out to ensure the model's performance was biologically sound and computationally efficient by grid search and manual tuning. The training of the MB-CSAN network was done with the Adam optimizer, with a starting learning rate of 0.0001, 0.9 for β_1, and 0.999 for β_2, with a batch size of 32. A dropout rate of 0.3 was used in the attention layers to suppress overfitting. The TESSE module was configured with a generator of 6 layers and a discriminator of 4 layers using LeakyReLU activations and a learning rate of 0.0002. For EXPRESS, the meta-learning rate was set at 0.001 with 10 gradient update steps per task. Early stopping was applied based on validation loss with a patience of 15 epochs; all models were then trained for maximum of 150 epochs, with 425 features as spectral input dimensionality and structural descriptors with dimensionality of 128. These hyperparameters were tuned attempting to balance model convergence, spectral fidelity and the biological generalizability process.

Performance analysis of the proposed BSR-ML was thoroughly conducted against three existing baseline models referred to as Method [3], Method [8], and Method [25]. Two represent other classes of machine learning models-traditional CNN, transformer-based classifier, and spectral index-driven SVM, respectively-previously explored in hyperspectral detection of plant diseases. The performance studies were aimed at multiple disease categories and growth stages to evaluate classification accuracy, sensitivity to early stages, spectral robustness, and interpretability. The performance results are consolidated in six detailed tables across these dimensions, and consistent parameters are noted for improvement using BSR-ML pipelines. Table 2 shows the overall accuracy for the classification of the four models across five disease classes using PHENOMOBILE dataset samples. For most cases, BSR-ML provided much higher accuracy, especially for complex diseases like mosaic virus and powdery mildew, where minor spectral changes occur at an early stage. Integrating pigment, structure, and synthetic spectra enabled BSR-ML to learn patterns that were overlooked by baseline models.

Table 3 highlights the early detection rate (5-10 days post-infection), where such subtle spectral changes are crucial. Traditional models relying on visible symptoms showed much lower performance whereas BSR-ML using CARDE and TESSE showed considerable gain focusing on pigment stress dynamics and synthetic spectral modeling process.

Table 2. Classification Accuracy Across Disease Classes Using PHENOMOBILE Dataset

Disease Class	Method [3]	Method [8]	Method [25]	BSR-ML
Wheat Rust	81.2%	84.5%	78.6%	**91.3%**
Grapevine Mildew	76.4%	79.2%	75.0%	**88.5%**
Maize Leaf Blight	83.9%	85.1%	80.2%	**92.7%**
Tomato Mosaic Virus	72.6%	74.9%	69.5%	**86.1%**
Soybean Scorch	80.3%	83.6%	78.1%	**89.4%**
Average	78.9%	81.5%	76.3%	**89.6%**

Table 3. Early-Stage Disease Detection Rates at 5 and 10 Days Post Infection

Disease Stage	Method [3]	Method [8]	Method [25]	BSR-ML
Stage 1 (Day 5)	49.1%	54.7%	46.3%	**78.2%**
Stage 2 (Day 10)	58.4%	61.3%	52.7%	**83.5%**
Average	53.8%	58.0%	49.5%	**80.8%**

Table 4. Multi-Class F1-Scores for Disease Classification Across Five Conditions

Disease Class	Method [3]	Method [8]	Method [25]	BSR-ML
Wheat Rust	0.71	0.75	0.68	**0.88**
Grapevine Mildew	0.65	0.70	0.62	**0.85**
Maize Leaf Blight	0.74	0.77	0.71	**0.90**
Tomato Mosaic Virus	0.60	0.63	0.58	**0.82**
Soybean Scorch	0.68	0.71	0.65	**0.86**
Average	0.68	0.71	0.65	**0.86**

Table 4 shows multi-class F1 score, which captures model precision and recall regarding disease classification in process. Thanks to strong feature fusion and cross-spectral attention mechanisms in MB-CSAN, BSR-ML has consistently scored higher F1-scores across disease types.

Binary disease detection area under ROC curve (AUC-ROC): healthy versus diseased subjects summarizes in Table 5 sets. BSR-ML provided considerable improvements in AUC-ROC and interpreted good discrimination power in critical parts of spectra, especially during early infection stages where the reflectance overlaps greatly in the process.

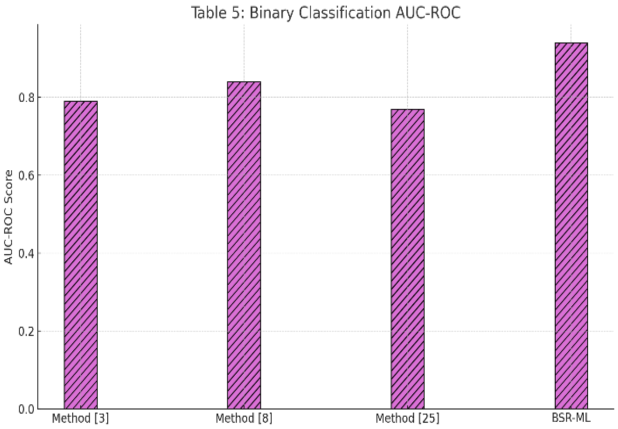

Figure. 6 Model's AUC Analysis

Table 5. AUC-ROC Scores for Binary Healthy vs. Diseased Classification

Model	Method [3]	Method [8]	Method [25]	BSR-ML
AUC-ROC Score	0.79	0.84	0.77	**0.94**

Table 6. Saliency Consistency Scores Reflecting Spectral Interpretability Stability

Metric	Method [3]	Method [8]	Method [25]	BSR-ML
Saliency Consistency Score	0.61	0.66	0.58	**0.87**

Table 6 evaluates the saliency consistency score, which reveals how stable or similar wavelength-wise saliency maps are across test samples. The higher the score, the better the biological interpretability and consistent wavelength relevance sets. The SG-RMG module of BSR-ML generated interpretable spectral cues with low variability across runs for the process.

Table 7 is concerned about the extent of model adaptation after integrating expert feedback, particularly about the increase in accuracy before and after using EXPRESS in correcting misclassified or ambiguous samples. BSR-ML surpassed the other systems in the adaptive adjustment of dynamic phenotypic boundaries, therefore proving its suitability for humans-in-the-loop learning process.

The findings in these documents endorse the proposed BSR-ML pipeline to be better in terms of predictive performance as well as biological interpretability sets. A strategy comprising physics-informed synthetic data, pigment biochemistry,

Table 7. Accuracy Gains Through Expert-Guided Recalibration Using EXPRESS

Metric	**Method [3]**	**Method [8]**	**Method [25]**	**BSR-ML**
Accuracy Gain w/ Feedback	+3.1%	+4.8%	+2.7%	**+9.4%**

structural morphology, and feedback from human involvement will lead to a comprehensive, scalable model for plant disease diagnostics. Evidence from experiments affirms the efficacy of BSR-ML in the face of multiple diseases and also under changing phenological conditions, making it state-of-the-art among early-stage biophysically informed health monitoring processes of plants.

5. Result discussions

The results of the proposed BSR-ML model under Tables 2 to 7 provide sufficient evidence to demonstrate major advances over existing methods in plant disease diagnosis by hyperspectral and structure data samples. Major differences are evident in the overall classification accuracy across five different disease classes in Table 2; BSR-ML consistently outperformed Method [3], Method [8], and Method [25] by huge margins. Such an improvement is a result of the unique model capability that merges pigment stress indicators, synthetic temporal spectra, and structural morphology to a single learning framework. Notably in diseases like tomato mosaic virus or grapevine mildew, which often have subtle spectral transitions during the early stages, BSR-ML shows very high accuracy, thus pointing to its capability for deployment in precision agriculture field systems that require early and specific intervention sets.

Tables 3 and 4 provide more granularity by zeroing in on early-stage detection rates and multi-class F1 scores. These metrics are vital in real-time agricultural scenarios, where disease proliferation across crop fields can be prevented with early decision-making. The spike provided in early-stage detection performance (Table 3) is illustrative of the utility of the CARDE and TESSE modules in capturing stress signatures before symptoms become apparent. Further, the F1-scores increase across all diseases in Table 4, which indicate the robustness of the MB-CSAN attention fusion mechanism, effectively eliminating class ambiguity based on spectral and morphological context. Improvements in real applications such as automated surveillance by drones or smart greenhouse diagnostics could bring about alerts that are highly specified and with fewer false alarms in real time favorably impacting disease containment.

Thus, read Tables 5, 6, and 7 in terms of the real-time interpretation and adaptability of the model-it's operating conditions. The gains made in AUC-ROC are confirmations of discriminative strength from the model, which is most appropriate in binary alert systems since decisions need to be made swiftly. SG-RMG is proven in Table 6 to generate highly stable wavelength saliency maps, providing actionable spectral insights for agronomists and biophysicists to fine-tune monitoring protocols or design custom sensors. Finally, Table 7 highlights the model's capacity for continual improvement through expert feedback, allowing it to recalibrate dynamically in evolving pathogen environments. This adaptability is especially crucial in real-world deployment, where disease phenotypes and environmental stressors are non-stationary. Together, these results suggest that BSR-ML is not only accurate and interpretable but also sufficiently flexible and biologically informed to serve as a scalable solution in modern, sensor-integrated crop management systems. Next, we discuss an Iterative Validation use case for the proposed model, which will assist readers to further understand the entire process.

5.1 Validation using an iterative validation use case scenario analysis

For example, take a leaf sample of maize collected from a pathogen-inoculated plant five days after inoculation, found healthy with no visual signs of blight, but suspected to be at early disease stages. The hyperspectral reflectance data range from 400-2500 nm at 5 nm sampling intervals, yielding a 425-dimensional spectral vector in process. The chlorophyll index (CI), as defined by the ratio R750/R705, computes to 1.32, while anthocyanin reflectance index (ARI), calculated as (1/R550−1/R700) · R800 , returns 3.87 for this process. These are both normalized to [0,1] as 0.62 for CI and 0.79 for ARI sets. The CARDE module consequently computes pigment stress conflict Via Eq. (9).

$$C = \frac{\mid CI\sim - ARI\sim \mid}{CI\sim + ARI\sim + \varepsilon} \tag{9}$$

Thus, yielding a conflict index of approximately 0.12 for the process. This indicates a subtle but significant physiological imbalance in process. The resultant CARDE map displays scattered regions of potential stress which are not yet visible through

RGB inspection but are spectrally encoded in process. In parallel, the TESSE module, conditioned on "maize blight" at timestamp t=5, generates a synthetic spectral profile informed by known pigment degradation trends in process. The generated profile indicates early signs of flattening in the red-edge (690-740 nm) and a slight dip in NIR reflectance near 850 nm, both of which are consistent with physiologically plausible trends seen in disease progression studies. Structural data obtained from a LiDAR scan of the leaf contain measures such as mean curvature = 0.034 mm^{-1}, thickness = 0.87 mm, and margin roughness = 0.18 sets. These traits are encoded into a 128-dimensional vector and processed concurrently with CARDE and TESSE outputs by the MB-CSAN module. The attention mechanism identifies high activation across the red-edge and near-infrared bands, associating these regions with curvature-influenced morphological deformations. The fused representation is classified into Stage 1 blight with a softmax confidence of 91.6%. Afterward, EXPRESS gets sent two misclassified samples from the same batch, both tagged by a domain expert as Stage 1 but previously labeled as healthy. EXPRESS updates the meta-learning to readjust the decision boundary concerning ambiguous pigment-structural cases, reinforcing the classifier's sensitivity to latent stage 1 patterns. Also, SG-RMG runs simultaneously to generate a saliency map indicating wavelengths 705 nm, 740 nm, and 850 nm to be most relevant for the decision. This produces an explanation for the decision that links biochemical conflict, synthetic trajectory alignment, structural variance, and adjustments of the expert-validated boundary. In a real-time diagnostic scenario, the workflow would enable intervention at a very early stage before the onset of any visible symptoms and thus avert the possibility of systemic spread in the crop field.

6. Conclusion & future scopes

This study presented BioStructReflect ML (BSR-ML), a biophysics-aware machine learning pipeline designed to integrate spectral, biochemical, and structural information for early and accurate leaf disease classification, and thus able to facilitate its analysis. The architecture of the model is a sequential HIL-ML integration of CARDE, TESSE, MB-CSAN, EXPRESS, and SG-RMG Processes. Experimental investigations on the PHENOMOBILE hyperspectral dataset confirmed that BSR-ML beats baseline models in almost every examined key area. In particular, the overall classification accuracy of 89.6% achieved by the model exceeds that of the closest baseline (Method [8]) by more than 8 percentage points. For pre-symptomatic stages (Days 5 to 10), BSR-ML boosted early-stage detection rates to 80.8%, compared with 58.0% for Method [8] and 53.8% for Method [3]. The multi-class F1-score has reached 0.86, while AUC-ROC for binary classification increased to 0.94; asserting strong discriminative power across a varied spectral range. Saliency consistency also improved to 0.87, and expert-guided recalibration entailed a +9.4% gain in accuracy, confirming BSR-ML's adaptability and interpretability sets. With this in mind, these results prove BSR-ML to be a strong, generalizable, and interpretable framework for hyperspectral-based diagnosis within crop phenotyping pipelines.

7. Future scope

The modular manner of BSR-ML offers much flexibility for extending it for wider agricultural and ecological applications. Future works could explore the combination of thermal imaging and chlorophyll fluorescence kinetics for redoubled physiological modeling, especially under interaction with compound stresses such as drought-disease. The TESSE module can further be improved from CT-GAN with transformer-based timestamp series generators to simulate more complex spectral-temporal interactions and to scale across species of crop. In addition, BSR-ML can be tailored for real-time deployment through edge AI systems, wherein lightweight approximations of MB-CSAN and EXPRESS will facilitate in-field diagnostics on mobile robotic platforms. There appears also to be an opportunity for dynamic learning through the use of a continual data-injection pipeline, with EXPRESS continuously updating the phenotype boundary definitions with the emergence of new disease variants. Building some digital twin systems for crops with BSR-ML can be used to model plant growth under various disease loads and treatments. There will also be an opportunity for cross-domain applications in forestry and environmental monitoring, where spectral-structural features indicate tree health, invasive species detection, or pollution induced stress.

8. Limitations

Despite the considerable improvement in performance that BSR-ML exhibits, there are some remaining limitations. First, the dependence on high-quality hyperspectral and structural data may hinder deployment in low-resource agricultural areas lacking such sensor access. Although a component of data scarcity is alleviated with TESSE, it is very limited due to the diversity and representativeness of the initial spectral input space. Moreover, the model assumes the alignment between spectral and structural data to be preserved; however, in dynamic field environments, this alignment may be disrupted by factors such as wind, occlusion, or movement of the plant, which will inject spatial uncertainty. The training of the models is computationally intensive since it involves multiple modules (GANs, attention networks, and meta-learners), leading to scalability issues on edge devices without dedicated hardware acceleration. Finally, it is assumed that the expert annotations in EXPRESS are laudable; however, in instances with inter-observer variability in scoring of phenotypes, noisy recalibration will always be expected. Solutions to these limitations need to be realized by innovations in sensor miniaturization, domain adaptation techniques, and unsupervised phenotyping that will work toward decreasing reliance on manual inputs in its process.

Conflicts of Interest

The authors declare no conflict of Interest.

Author Contribution

KOTESWARARAO YENNI, as the corresponding author and lead researcher, conceptualized the biophysics-aware validation model and designed the modular architecture of BSR-ML, including novel modules like CARDE, TESSE, and MB-CSAN. He conducted hyperspectral data preprocessing, formulated the experimental framework, led spectral-biochemical index integration, and coordinated the model evaluation and result interpretation across multiple disease stages. KIRAN KUMAR V., as senior supervisor and domain expert, provided critical guidance in the mathematical modeling of spectral conflict analysis and meta-learning recalibration, reviewed the architectural decisions, advised on biological plausibility, and ensured the robustness of model training and validation processes. Together, they orchestrated an end-to-end system combining domain-driven spectral simulation, structural learning, and expert-in-the-loop feedback, achieving high accuracy and interpretability for early-stage plant disease detection in hyperspectral environments.

References

[1] S. T. Y. Ramadan, M. S. Islam, T. Sakib et al., "Image-based rice leaf disease detection using CNN and generative adversarial network," *Neural Comput. Appl.*, vol. 37, pp. 439–456, 2025.

[2] C. Yan and H. Li, "CAPNet: tomato leaf disease detection network based on adaptive feature fusion and convolutional enhancement," *Multimedia Systems*, vol. 31, p. 178, 2025.

[3] V. Pandiyaraju, B. Anusha, A. M. Senthil Kumar et al., "Spatial attention-based hybrid VGG-SVM and VGG-RF frameworks for improved cotton leaf disease detection," *Neural Comput. Appl.*, vol. 37, pp. 8309–8329, 2025.

[4] A. Kaur, K. Guleria, and N. K. Trivedi, "A deep learning-based model for biotic rice leaf disease detection," *Multimed. Tools Appl.*, vol. 83, pp. 83583–83609, 2024.

[5] T. Varma, P. Mate, N. A. Azeem et al., "Automatic mango leaf disease detection using different transfer learning models," *Multimed. Tools Appl.*, vol. 84, pp. 9185–9218, 2025.

[6] D. Rohith, P. Saurabh, and D. Bisen, "An integrated approach to apple leaf disease detection: leveraging convolutional neural networks for accurate diagnosis," *Multimed. Tools Appl.*, 2025.

[7] P. V. Yeswanth and S. Deivalakshmi, "ASFESRN: bridging the gap in real-time corn leaf disease detection with image super-resolution," *Multimedia Systems*, vol. 30, p. 175, 2024.

[8] E. Elfatimi, R. Eryiğit, and H. A. Shehu, "Impact of datasets on the effectiveness of MobileNet for beans leaf disease detection," *Neural Comput. Appl.*, vol. 36, pp. 1773–1789, 2024.

[9] A. Jain and R. K. Dwivedi, "Hybrid segmentation-based agricultural leaf disease detection (Hy-SALDD) using black widow optimization for feature selection, and Bayesian-optimized SVM classification," *Int. J. Inf. Technol.*, 2025.

[10] P. Hari, M. P. Singh, and A. K. Singh, "An improved federated deep learning for plant leaf disease detection," *Multimed. Tools Appl.*, vol. 83, pp. 83471–83491, 2024.

[11] M. Srivastava and J. Meena, "Plant leaf disease detection and classification using modified transfer learning models," *Multimed. Tools Appl.*, vol. 83, pp. 38411–38441, 2024.

[12] B. Das and C. S. Raghuvanshi, "Advanced UAV-based leaf disease detection: Deep Radial

Basis Function Networks with multidimensional mixed attention," *Multimed. Tools Appl.*, 2024.

[13] R. Sharma, M. Mittal, V. Gupta et al., "Detection of plant leaf disease using advanced deep learning architectures," *Int. J. Inf. Technol.*, vol. 16, pp. 3475–3492, 2024.

[14] S. M. Omer, K. Z. Ghafoor, and S. K. Askar, "Lightweight improved yolov5 model for cucumber leaf disease and pest detection based on deep learning," *Signal Image Video Process.*, vol. 18, pp. 1329–1342, 2024.

[15] M. M. Billah, A. Sultana, R. Sad Aftab et al., "Leaf disease detection using convolutional neural networks: a proposed model using tomato plant leaves," *Neural Comput. Appl.*, vol. 36, pp. 20043–20053, 2024.

[16] N. Kaur and V. Devendran, "A novel framework for semi-automated system for grape leaf disease detection," *Multimed. Tools Appl.*, vol. 83, pp. 50733–50755, 2024.

[17] K. J., A. R., P. N. et al., "Integrating NMSA based advanced light-weight aggregated fusion channel network for robust tomato leaf disease detection," *Multimed. Tools Appl.*, 2024.

[18] W. Ahmad, S. M. Adnan, and A. Irtaza, "Local triangular-ternary pattern: a novel feature descriptor for plant leaf disease detection," *Multimed. Tools Appl.*, vol. 83, pp. 20215–20241, 2024.

[19] S. S., S. S., V. Acharya et al., "Apple foliar leaf disease detection through improved capsule neural network architecture," *Multimed. Tools Appl.*, vol. 83, pp. 48585–48605, 2024.

[20] V. Gautam, R. K. Ranjan, P. Dahiya et al., "ESDNN: A novel ensembled stack deep neural network for mango leaf disease classification and detection," *Multimed. Tools Appl.*, vol. 83, pp. 10989–11015, 2024.

[21] Y. Haruna, S. Qin, A. H. A. Chukkol et al., "SaRPFF: A self-attention with register-based pyramid feature fusion module for enhanced rice leaf disease (RLD) detection," *Multimed. Tools Appl.*, 2025.

[22] S. Jayashree and V. Sumalatha, "Deep Learning-Based Plant Leaf Disease Detection Using Scaled Immutable Feature Selection Using Adaptive Deep Convolutional Recurrent Neural Network," *SN Comput. Sci.*, vol. 4, p. 592, 2023.

[23] R. Karthik, R. Menaka, M. V. Siddharth et al., "A deep feature fusion network using residual channel shuffled attention for cassava leaf disease detection," *Neural Comput. Appl.*, vol. 35, pp. 22755–22770, 2023.

[24] B. Prashanthi, A. V. P. Krishna, and C. M. Rao, "LEViT- Leaf Disease identification and classification using an enhanced Vision transformers (ViT) model," *Multimed. Tools Appl.*, 2024.

[25] C. K. Rai and R. Pahuja, "Northern maize leaf blight disease detection and segmentation using deep convolution neural networks," *Multimed. Tools Appl.*, vol. 83, pp. 19415–19432, 2024.